Polarization observables in $\vec{\pi d}$ elastic scattering: Analyzing powers τ_{22} and iT_{11}

C. R. Ottermann, E. T. Boschitz, H. Garcilazo, W. Gyles, W. List,
R. Tacik, and M. Wessler
Kernforschungszentrum Karlsruhe, Institut für Kernphysik and Institut für Experimentelle Kernphysik, der Universität Karlsruhe, D-7500 Karlsruhe, Federal Republic of Germany

S. Mango, B. van den Brandt, and J. A. Konter
Schweizerisches Institut für Nuklearforschung, CH-5234 Villigen, Switzerland

E. L. Mathie
University of Regina, Regina, Saskatchewan, Canada S4S 0A2
(Received 1 June 1988)

The composite spin observable $\tau_{22} \equiv (T_{22} + T_{20}/\sqrt{6})$ has been measured at five incident pion energies between 134 and 294 MeV, in an angular range between 90° and 170°, using a tensor-polarized deuterium target. New, accurate data for the vector analyzing power iT_{11} were obtained at the same time. In combination with the results reported in part I of this series, our measurements allow us to determine the three analyzing powers T_{20}, T_{21}, and T_{22}, separately, and compare them with existing theoretical calculations, all of which fail, in one way or another, to reproduce the entire data set.

I. INTRODUCTION

There are four polarization observables which can be measured in the $\vec{\pi d} \rightarrow \pi d$ elastic scattering reaction, using a pion beam and a polarized deuterium target. These are the vector analyzing power iT_{11}, and the tensor analyzing powers T_{20}, T_{21}, and T_{22}. Unfortunately, these last two (T_{21} and T_{22}) cannot be measured separately, but only as linear combinations involving the other tensor observables. The general motivation for our group's systematic study of the πd elastic scattering reaction, in the energy region of the $\Delta(3,3)$ resonance, has already been given in part I of this paper.[1] There, we presented results for T_{20}, and the "composite" observable $\tau_{21} \equiv T_{21} + \frac{1}{2}[T_{22} + (T_{20}/\sqrt{6})]$. In this part, we present results for another "composite" observable, $\tau_{22} \equiv T_{22} + (T_{20}/\sqrt{6})$. Part I of this paper contained a very detailed discussion of the experimental procedure and the data analysis techniques which were employed in order to extract the values of the polarization observables from the measured cross sections. With the knowledge of T_{20} and the two composite observables τ_{21} and τ_{22}, we are now able to determine the values of all three tensor analyzing powers T_{20}, T_{21}, and T_{22}. Thus, this part of the paper contains a more detailed comparison of the polarization observables with various theoretical calculations.

At the same time as we measured τ_{22}, we obtained results for iT_{11}, and these are also presented in this part of the paper. On one hand, the fact that both observables are measured together presents a difficulty, because the separation of τ_{22} from iT_{11} requires comparable positive and negative vector polarizations of the deuterium target. On the other hand, the fact that the vector polarization of the target was almost a factor of 3 larger than the one available in our earlier measurements[2] means that the values of iT_{11} we have obtained are very precise. The precision is in fact comparable to that of the best available πd differential cross sections. Thus, the new results have a significant impact on the amplitude analysis of the reaction, which will be presented in part III of this paper.[3]

II. THE EXPERIMENT

For the measurements of τ_{22} and iT_{11} presented here, the polarized target magnetic field direction, which is also the direction of the deuteron's spin quantization axis, was perpendicular to the scattering plane. That is, the angles α and β, defined in part I of this paper,[1] were 90° and 0°, respectively. In this case, the general expression for a polarized cross section is

$$\sigma^{\mathrm{pol}} = \sigma^{\pm} = \sigma^{0} \left[1 \pm \sqrt{3} p_z i T_{11} - \frac{\sqrt{3}}{2} p_{zz} \left[T_{22} + \frac{T_{20}}{\sqrt{6}} \right] \right] . \tag{1}$$

It is evident that iT_{11} can be obtained from the difference of the ratios σ^{+}/σ^{0} and σ^{-}/σ^{0}, while $\tau_{22} \equiv T_{22} + (T_{20}/\sqrt{6})$ can be obtained simultaneously from their sum.

For the measurements of T_{20} and τ_{21}, described in part I of this paper, the target magnetic field direction was such that the outgoing pions and deuterons were deflected out of the horizontal plane. This necessitated an appropriate adjustment of the vertical positions of the counters used. The present configuration has the advantage that the pion and deuteron counters could remain in

the horizontal plane. The actual angles at which the particles are detected, however, are not the same as those with which they scattered, due to the effect of the target magnetic field. The relations between the two sets of angles were determined using ray-trace calculations, which included detailed simulation of particle energy losses in the target material. These calculations were checked experimentally by maximizing the πd coincidence count rate with the pion counters held fixed, and the associated deuteron counters moved to either side of their nominal positions. Agreement was always found, to within 0.5°, between the calculated and experimentally determined angles.

The polarized target was operated in "frozen spin mode," as described in part I of this paper, but at the normal magnetic field value of $B=2.5$ T, rather than a reduced "holding field" as was the case for the T_{20} and τ_{21} measurements. At this normal field value, the target polarization decays much more slowly than at the reduced field value. The ratio $p_z(t)/p_z(0)$ is plotted as a function of time in Fig. 1. An exponential curve fit to the data gives a mean decay time of $\tau=400$ h. Performing the experiment with a target magnetic field of 2.5 T also enabled us to extend the measurements to larger pion angles than would otherwise have been possible. This is because the outgoing pions were deflected away from the incident beam.

The measured cross sections σ^+, σ^-, and σ^0 were determined with a high statistical accuracy, typically $\Delta\sigma/\sigma=0.7\%$. Thus, the biggest uncertainty in the determination of τ_{22} comes from the determination of the relative positive and negative target polarizations. Therefore, special attention was paid to the NMR system in order to obtain signals which were very similar in shape. A typical pair of signals is shown in Fig. 2. The uncertainty in the relative determination of p_z^+ and p_z^- was typically $\pm 2.5\%$.

The data reduction procedure used to extract values of τ_{22} and iT_{11} from the measured cross sections was similar to the one discussed extensively for the T_{20} and τ_{21} measurements in part I of this paper. In particular, the polarization observables were determined using the "fitting" and "matrix" methods. An example of the fitting method is shown for two angles at $T_\pi=256$ MeV in Fig. 3. In

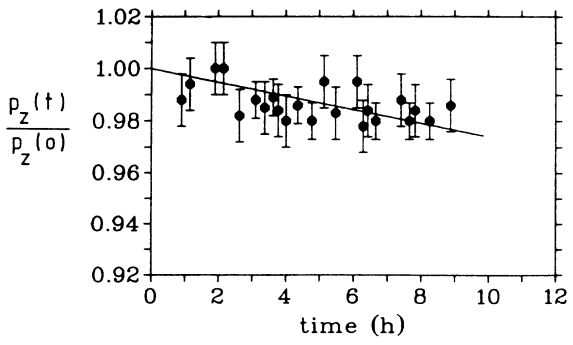

FIG. 1. Decay of the target polarization in frozen spin mode. The line represents an exponential fit to the polarization values p_z.

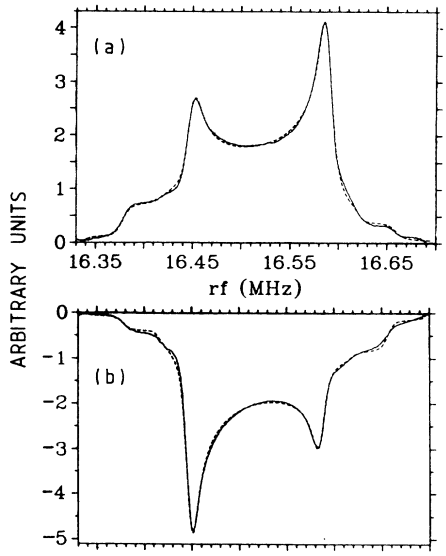

FIG. 2. Typical (a) negative ($p_z=-0.482$) and (b) positive ($p_z=0.417$) dynamically enhanced NMR signals. The solid lines represent measured spectra, the dashed lines are the result of a fitting procedure.

Fig. 3(a), there is a large difference between σ^+ and σ^-. The result is $iT_{11}=0.40\pm0.15$ and $\tau_{22}=-0.61\pm0.13$. In Fig. 3(b), the difference is small, and the result is $iT_{11}=0.06\pm0.01$ and $\tau_{22}=-0.45\pm0.08$.

In part I of this paper, we described how we could use our various methods of analysis to test for possible misalignments of the target magnet, and errors in the

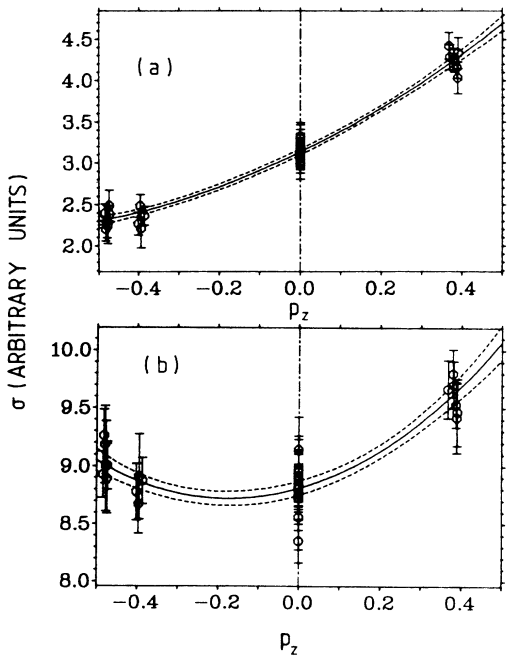

FIG. 3. Examples of the fitting method used to extract values of iT_{11} and τ_{22} from the measured σ^+, σ^0, and σ^- cross sections. The solid lines represent the best fit, and the dashed lines the associated error band. (a) is for $\theta_\pi=134°$, and (b) is for $\theta_\pi=75.5°$, both at $T_\pi=256$ MeV.

determination of the target polarization. This is no longer possible for iT_{11} and τ_{22}. It can be shown though, that as long as the angular misalignments $\Delta\alpha$ and $\Delta\beta$ are smaller than 1° (which was the case in our experiment), the misalignment error can be neglected. The present results (particularly τ_{22}) are still sensitive to systematic errors in the determination of the relative values of the positive and negative target polarizations. This is illustrated in Fig. 4, where the results at $T_\pi = 256$ MeV are shown. The statistical errors are represented by the thin lines, while the systematic errors are indicated by the solid bars. These were obtained by varying the positive and negative target polarizations from their best fit values by $\pm 2.5\%$, and recalculating iT_{11} and τ_{22}. As one can see, the systematic errors in τ_{22} increase considerably with the magnitude of iT_{11}.

The results of iT_{11} and τ_{22} from this experiment are listed in Table I for the five energies between 134 and 294 MeV at which data were obtained. The errors quoted are both the statistical uncertainties, and the systematic ones arising from the error in the determination of the relative positive and negative target polarizations. In addition,

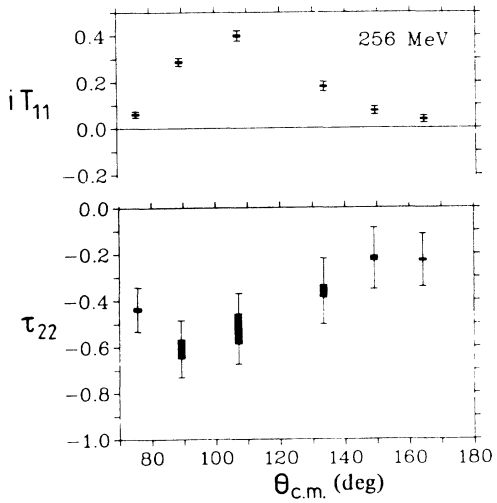

FIG. 4. Results for iT_{11} and τ_{22} at $T_\pi = 256$ MeV. The thin lines represent the statistical errors, while the solid bars represent the systematic errors. These are due to the uncertainty in the determination of the relative negative and positive target polarizations.

TABLE I. Results for iT_{11} and τ_{22} from the present experiment. The statistical and systematic uncertainties are quoted separately. The normalization uncertainties are 4% for iT_{11} and 8% for τ_{22}.

		iT_{11}			τ_{22}		
T_π (MeV)	$\theta_{c.m.}$	value	stat.	syst.	value	stat.	syst.
134	112.2	0.234	0.015	0.002	−0.197	0.126	0.043
	126.9	0.168	0.014	0.002	−0.186	0.115	0.030
	138.7	0.134	0.010	0.002	−0.139	0.094	0.023
	150.3	0.084	0.010	0.002	−0.357	0.082	0.013
	161.5	0.063	0.010	0.002	−0.248	0.084	0.010
	170.4	0.028	0.010	0.001	−0.092	0.097	0.004
180	108.1	0.370	0.012	0.003	−0.430	0.081	0.059
	125.2	0.274	0.010	0.003	−0.393	0.078	0.043
	137.0	0.232	0.013	0.003	−0.374	0.094	0.035
	146.1	0.174	0.012	0.003	−0.329	0.085	0.027
	157.3	0.133	0.016	0.003	−0.395	0.105	0.021
	168.3	0.068	0.018	0.004	−0.457	0.126	0.010
219	86.3	0.351	0.017	0.005	−0.503	0.152	0.060
	104.4	0.382	0.018	0.005	−0.513	0.142	0.066
	126.4	0.247	0.016	0.004	−0.404	0.133	0.043
	142.6	0.163	0.017	0.005	−0.537	0.152	0.027
	153.7	0.092	0.017	0.005	−0.571	0.159	0.016
	166.7	0.043	0.018	0.004	−0.510	0.162	0.008
256	75.7	0.061	0.013	0.004	−0.437	0.095	0.008
	89.2	0.288	0.017	0.004	−0.608	0.123	0.041
	107.1	0.400	0.022	0.005	−0.522	0.152	0.064
	133.4	0.181	0.021	0.004	−0.361	0.142	0.026
	149.1	0.075	0.017	0.003	−0.219	0.133	0.010
	164.2	0.037	0.016	0.003	−0.228	0.114	0.004
294	77.3	−0.123	0.019	0.003	−0.408	0.120	0.026
	93.4	0.313	0.036	0.006	−0.721	0.224	0.053
	111.1	0.376	0.037	0.005	−0.371	0.227	0.070
	127.8	0.194	0.028	0.005	−0.510	0.172	0.033
	145.8	0.023	0.029	0.003	−0.352	0.190	0.007
	163.0	−0.004	0.023	0.003	−0.399	0.148	0.003

there is a normalization uncertainty for the entire data set, arising from the uncertainty in the determination of the absolute target polarization. This is 4% for the iT_{11} data (coming from Δp_z), and 8% for τ_{22} (coming from Δp_{zz}).

III. RESULTS AND DISCUSSION

A. Consistency check of the data

For several years there has been an experimental controversy over two sets of t_{20}^{lab} data for πd elastic scattering. One group of LAMPF obtained a smooth behavior of t_{20}^{lab} as a function of scattering angle and pion bombarding energy.[4,5] Another group, at Swiss Institute of Nuclear Research (SIN), found t_{20}^{lab} values which were of the opposite sign, and varied greatly with scattering angle and energy.[6] This controversy was finally resolved in favor of the LAMPF measurements by a third measurement of t_{20}^{lab} at TRIUMF,[7] and by a first measurement of T_{20}.[8] It thus seems appropriate to demonstrate that the data on T_{20} and τ_{21} presented in part I of this paper,[1] and the τ_{22} and iT_{11} data presented here, are self-consistent, and in agreement with the LAMPF results on t_{20}^{lab} (Ref. 5) and earlier data on iT_{11}.[2]

In Fig. 5 we compare the new iT_{11} data with those accumulated over several years in experiments where the target vector polarization was considerably smaller than the one available to us now.[2] Within the large errors of the previous measurements, there is consistency between the two data sets. At 180 and 219 MeV, however, the new data do seem to be systematically larger than the old. This may be due to the larger uncertainties associated with the determination of the absolute values of the target polarizations in some of the earlier measurements. At 134 MeV, the smooth angular dependence of iT_{11} beyond 110° is confirmed.

We have fit the angular distributions of T_{20}, τ_{21}, and τ_{22} at both 256 and 294 MeV with a series of Legendre polynomials. Using these fits, we can extrapolate the value of each of the measured observables to 180°. Since T_{21} and T_{22} are zero at 180°, we have that $\tau_{21}(180°) = \tau_{22}/2(180°) = T_{20}/2\sqrt{6}(180°)$, and thus the three values can be compared directly. The results are presented in Table II. It is evident that there is consistency between the measurements, which were made with completely different configurations for the polarized target and the πd counters. Recall that the quantization axis of the polarized deuteron target was perpendicular to the scattering plane for the τ_{22} measurement, collinear with the pion beam in the case of the T_{20} measurement, and at 45° to the incident pion beam for the τ_{21} measurement.

Since we found consistency between the measurements, we redid the Legendre polynomial fits, including the mean value of the extrapolated point at 180° along with the measured quantities. In Fig. 6, the results of these fits are shown, including the uncertainties in the fitted coefficients, as shaded bands. With these fits, we can determine the tensor analyzing powers T_{20}, T_{21}, and T_{22}, from the measured composite observables. They can also be used to obtain values for the tensor polarizations t_{20}^{lab}, t_{21}^{lab}, and t_{22}^{lab}. The various observables are related in the following way (see the Appendix for more details):

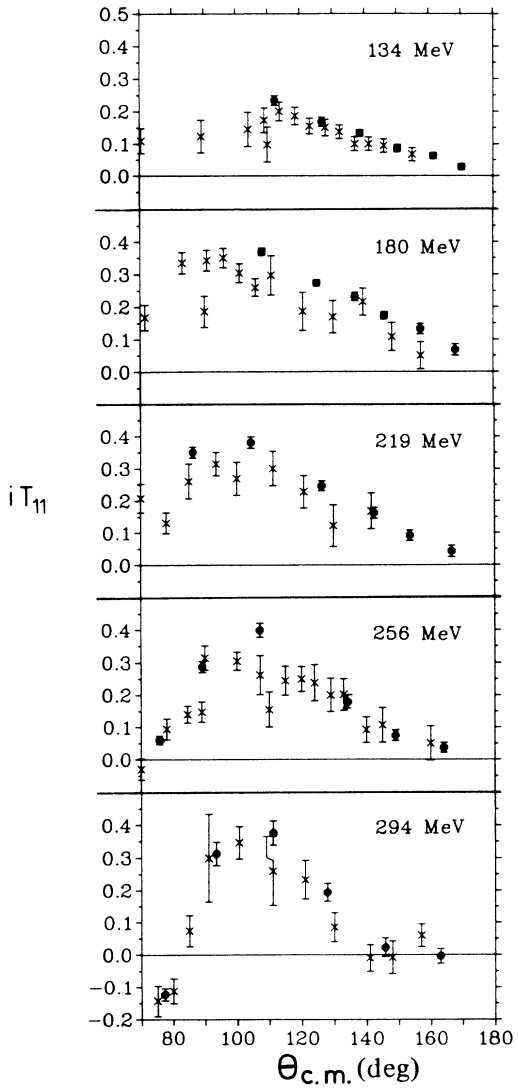

FIG. 5. Present result for iT_{11} (solid circles) in comparison with our previous measurements (Ref. 2), which were performed with much smaller target polarizations.

TABLE II. Values of $T_{20}/2\sqrt{6}$ at 180°, taken from the extrapolation of the Legendre polynomial fits to the measured values of T_{20}, τ_{21}, and τ_{22}.

T_π (MeV)	$T_{20}/2\sqrt{6}$	τ_{21}	τ_{22}	mean
256	−0.155±0.024	−0.180±0.108	−0.109±0.070	−0.151±0.022
294	−0.171±0.022	−0.251±0.105	−0.171±0.076	−0.174±0.021

$$\begin{bmatrix} T_{20} \\ T_{21} \\ T_{22} \end{bmatrix} = \begin{bmatrix} 1 & 0 & 0 \\ 0 & 1 & -\frac{1}{2} \\ -\frac{1}{\sqrt{6}} & 0 & 1 \end{bmatrix} \begin{bmatrix} T_{20} \\ \tau_{21} \\ \tau_{22} \end{bmatrix}, \tag{2}$$

$$\begin{bmatrix} t_{20} \\ t_{21} \\ t_{22} \end{bmatrix}^{\text{lab}} = \begin{bmatrix} \frac{3\cos^2\theta_R - 1}{2} & 2\sqrt{3/2}\sin\theta_R\cos\theta_R & \sqrt{3/2}\sin^2\theta_R \\ \sqrt{3/2}\sin\theta_R\cos\theta_R & 1-2\cos^2\theta_R & -\sin\theta_R\cos\theta_R \\ \frac{1}{2}\sqrt{3/2}\sin^2\theta_R & -\sin\theta_R\cos\theta_R & \frac{1+\cos^2\theta_R}{2} \end{bmatrix} \begin{bmatrix} T_{20} \\ T_{21} \\ T_{22} \end{bmatrix}. \tag{3}$$

The values for t_{20}^{lab}, t_{21}^{lab}, and t_{22}^{lab}, at 256 MeV, obtained from the fits illustrated in Fig. 6 are indicated by the shaded bands in Fig. 7. The data points for t_{20}^{lab} are from Ungricht *et al.*[5] The excellent agreement is very gratifying. It demonstrates consistency between completely different measurements. The tensor polarizations t_{21}^{lab} and t_{22}^{lab} are rather featureless in the sense that the polarization is close to zero over a large angular range. Similar results are obtained at 294 MeV.

One final obvious test consisted of comparing our results for T_{20} with the results of corresponding measurements made at TRIUMF.[9] The two sets of data agree very well except for one point, which may be considered some kind of statistical "odd ball." This datum ($T_{20} = -1.42 \pm 0.18$ at $\theta_{\text{c.m.}} = 167.2°$) is larger, by a factor of 2, than our data at $\theta_{\text{c.m.}} = 161.2°$ and 171.7°. It also disagrees with our τ_{21} and τ_{22} data extrapolated to 180° (see Table II).

B. Comparison with theoretical predictions

In Fig. 8 we compare our present iT_{11} data with the theoretical predictions from the Lyon group[10] (dot-dashed curves), the Flinders group[11] (dashed curve), Garcilazo[12] (solid curve), and the Hannover group[13] (dotted curve). It is evident that, faced with the precision of the present data, all theories fail, in one way or another, over the full energy range.

The experimental results for the measured observable τ_{22} are displayed in Fig. 9 together with theoretical pre-

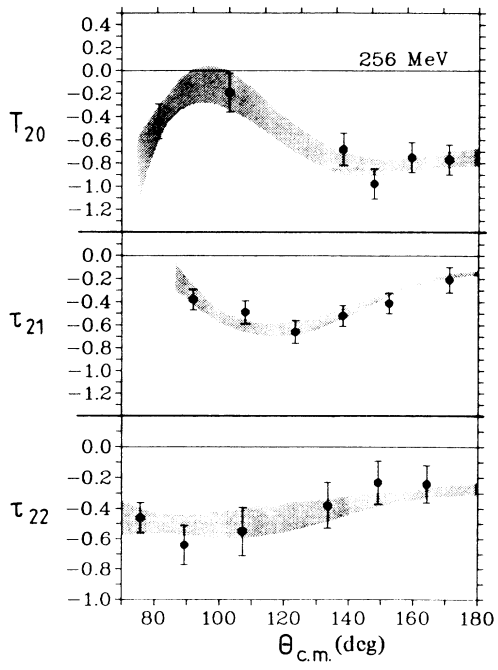

FIG. 6. Present results for τ_{22} at $T_\pi = 256$ MeV, along with the results for T_{20} and τ_{21} from part I of this paper (Ref. 1). The shaded bands represent the results of a Legendre polynomial fit to the data, which included the mean of the values extrapolated to 180° as one of the fitted points.

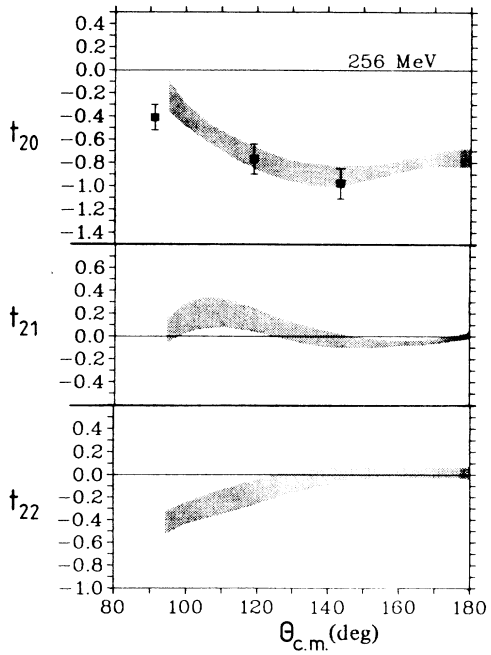

FIG. 7. The shaded bands represent values of t_{20}^{lab}, t_{21}^{lab}, and t_{22}^{lab} determined from a fit to our measured values of T_{20}, τ_{21}, and τ_{22}. The data points are from Ref. 5.

dictions from the same theory groups mentioned above. The labeling of the curves is the same as in Fig. 8. Below the (3,3) resonance the theoretical predictions do not differ very much. At higher energies there are pronounced discrepancies. With the exception of 256 MeV Garcilazo's predictions are in good agreement with the data. At this particular energy the predictions from the Lyon and Flinders groups follow the data. One should remember, however, that τ_{22} is a composite observable, and a comparison of this data with theory may lead to wrong conclusions. For example, the good agreement of the Flinders group with the τ_{22} data arises from an accidental cancellation, resulting from an over prediction of T_{20} (see preceeding paper[1]) and an under prediction of T_{22}.

Note that we have not presented a comparison of our data with predictions from all possible theory groups. For example, we do not show the calculations from the Weizman group[14] because their predictions are quite similar to those from the Flinders group.[11] We also do not show predictions from the Argonne group. Their recent model,[15] which has considerably advanced from the original work of Betz and Lee,[15] is quite similar to the one from the Hannover group.[13] However, there seem to be some unexplained problems in both calculations which lead to quite different predictions for $d\sigma/d\Omega$, iT_{11}, and t_{20}^{lab}. The differential cross section and the vector analyzing power are better predicted by the Hannover group, while there are problems for t_{20}^{lab} at large angles and higher pion energies. The predictions of t_{20}^{lab} by the Argonne group, on the other hand, agree well with all standard three-body calculations which have small effects from the P_{11} πN amplitude. It would be very desirable to see the inconsistencies between the Hannover and Argonne groups resolved.

C. The P_{11} problem

In the course of developing a unified theory of the NN-πNN system it was realized that a conventional

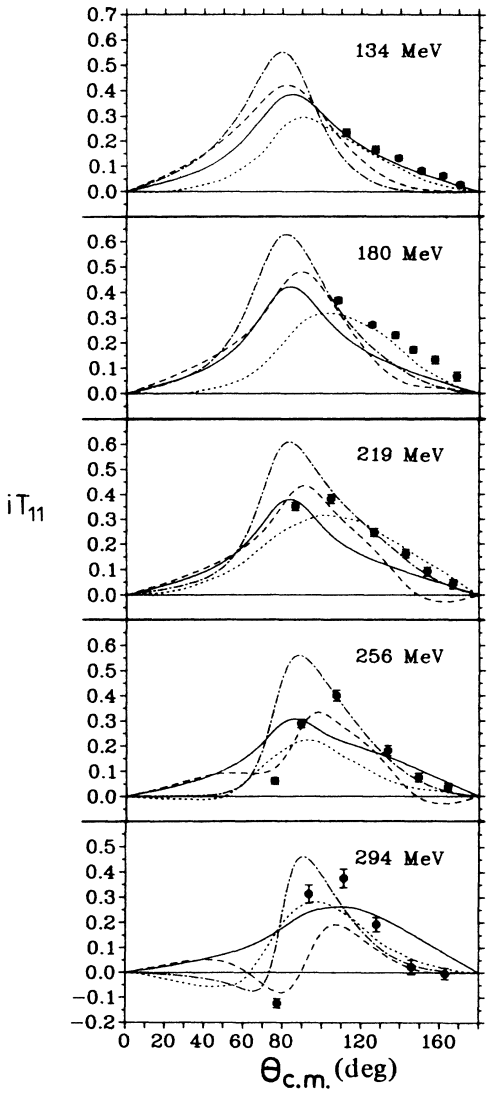

FIG. 8. Present results for iT_{11}, compared with theoretical predictions from the Lyon group (Ref. 10) (dot-dashed curves), the Flinders group (Ref. 11) (dashed curves), Garcilazo (Ref. 12) (solid curves), and the Hannover group (Ref. 13) (dotted curves).

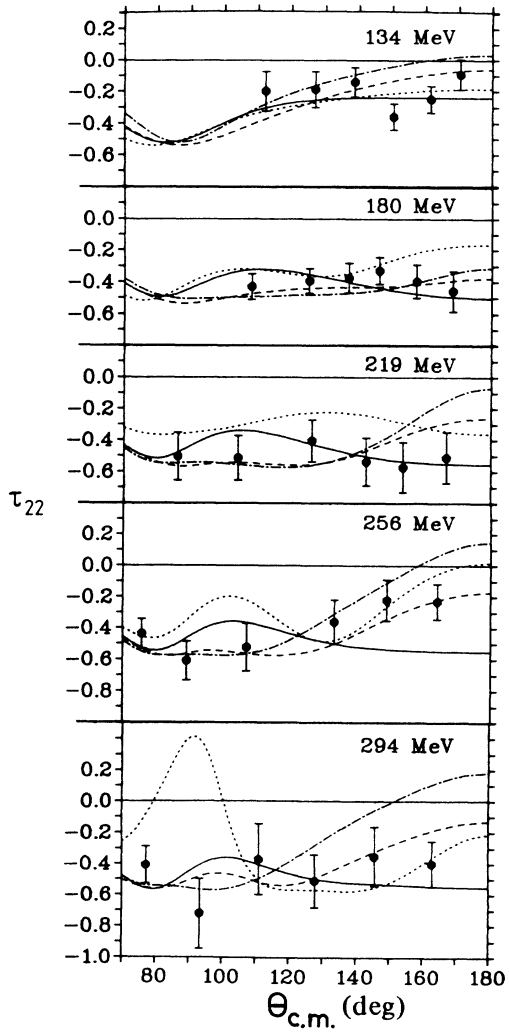

FIG. 9. Experimental results for τ_{22}. The curves are labeled as in Fig. 8.

three-body theory (for instance of the Faddeev type) is not enough to couple πd elastic scattering to the two-nucleon channel since absorption on one nucleon followed by the emission by the other nucleon is not a two-body process. To solve this problem, the most widely used procedure was to incorporate the P_{11} πN interaction in the theory in the following way. The total P_{11} t matrix was divided into an absorption part, due to the nucleon pole, and a rescattering part. Each part had to be large, of opposite sign and about equal in magnitude to reproduce the small on-shell P_{11} phase shifts up to pion energies of 300 MeV. This theoretical approach remained unchallenged, until the t_{20}^{lab} measurements from Ungricht *et al.*[5] demonstrated that there were problems with this treatment of the P_{11} amplitude. None of the theoretical predictions from the groups which split the P_{11} t matrix in the described way agreed with the experiment. On the other hand, if the P_{11} amplitude was omitted all together, the theoretical predictions agreed amongst themselves, and with the data. The authors of the t_{20}^{lab} measurement concluded that the theories described pion absorption incorrectly.

However, the large effects from pion absorption produced by some of those calculations are due to the particular way in which they split the P_{11} channel into pole and nonpole parts so that both parts are large, even though the on-shell P_{11} amplitude is rather small. This has nothing to do with the contribution of pion absorption itself, nor with the size of the effects produced by the intermediate nucleon-nucleon channels. For example, the calculation of Ref. 17 includes the coupling to the nucleon-nucleon channel in such a way that the elastic πd channel and the cross section for the reaction $\pi d \rightarrow NN$ are reproduced at the same time. Moreover, in that theory, the two nucleons in the intermediate state are allowed to interact with each other through the full nucleon-nucleon interaction represented by the Paris potential, so that very drastic variations are introduced in the part of the wave function describing the NN channels. The net effect, however, in the observables of the πd elastic reaction, is quite small.

The sensitivity of the treatment of the P_{11} πN amplitude was investigated by Afnan and McLeod.[18] They showed that quite different predictions for the πd elastic cross section, the vector polarization iT_{11}, and the tensor polarization t_{20}^{lab}, are obtained for different parametrizations of the P_{11} amplitude. Due to the Pauli principle the delicate cancellation between pole and nonpole terms required to give the proper πN on-shell behavior can be suppressed in the intermediate NN state for certain πd elastic partial waves. It is this "Pauli blocking" which makes some observables in the backward hemisphere very sensitive to the P_{11} splitting. So far, most of the unitary few-body models had relatively large contributions from the pole and the nonpole terms. The comparison with the t_{20}^{lab} data indicated, however, that both pieces should be small. This indeed has recently been proposed by Garcilazo[12] who quite successfully described the t_{20}^{lab} data at several energies. In addition, a global agreement was obtained with the experimental differential cross sections and the vector analyzing power measurements published so far.

It is interesting to compare our new experimental results on the four tensor observables with theoretical predictions in which the P_{11} amplitude is both included and omitted, in order to find which observable is most sensitive to the P_{11} treatment. In Figs. 10 and 11 we show our results for iT_{11}, T_{20}, T_{21}, and T_{22}, at 256 and 294 MeV, together with the theoretical predictions from Blankleider and Afnan.[11] The dashed curves represent the results of their complete calculation, while the dot-dashed curves show their results with the P_{11} amplitude left out. Being able, for the first time, to study the c.m. tensor observables T_{20}, T_{21}, T_{22} separately (not in the linear combination of t_{20}^{lab}), we notice that T_{21} and T_{22} are not very critical for the P_{11} problem. On the other hand, there are large differences between the two predictions, and with the data, for iT_{11} and T_{20}. These observables cannot be reproduced simultaneously. Noticing that the theoretical variations in T_{20} are extreme at 180° we extrapolated our

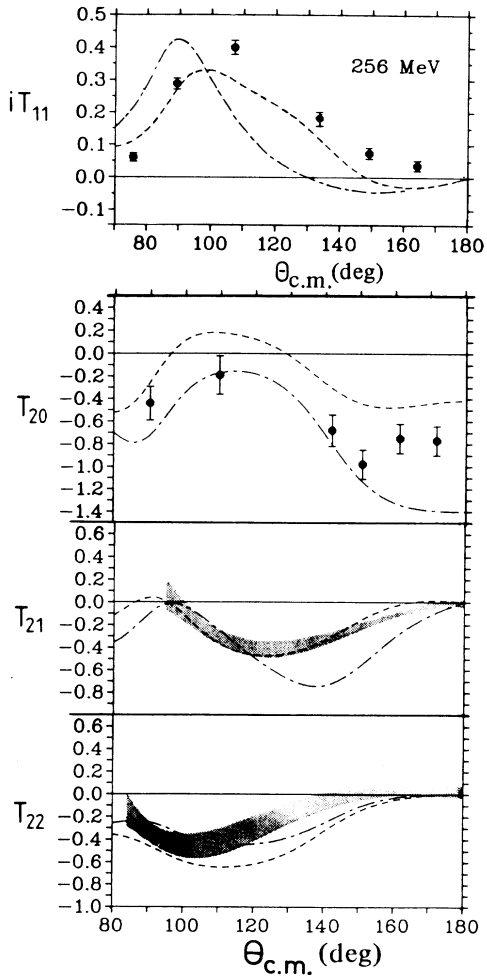

FIG. 10. Experimental results for iT_{11}, T_{20} (solid circles), and T_{21}, T_{22} (shaded bands) at $T_\pi = 256$ MeV. The dashed and dot-dashed curves are the theoretical predictions of Ref. 11, with and without the P_{11} amplitude, respectively.

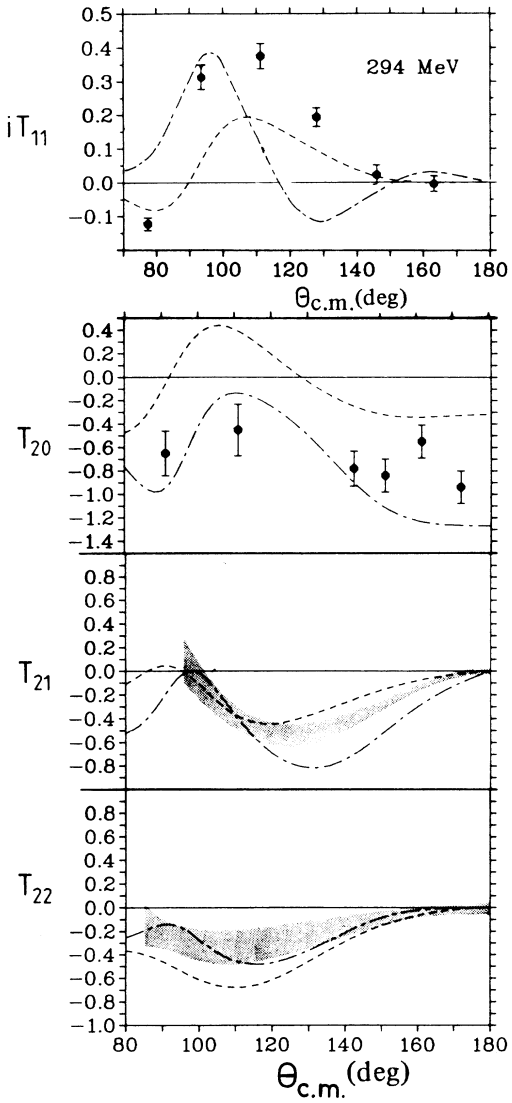

FIG. 11. Same as Fig. 10, but for $T_\pi = 294$ MeV.

T_{20}, τ_{21}, and τ_{22} data to 180° (remember that τ_{21} and τ_{22} at 180° are $T_{20}/2\sqrt{6}$ and $T_{20}/\sqrt{6}$, respectively). The values obtained are listed in Table III. Together with the extrapolation of the T_{20} measurement at 134 Mev (Ref. 8) and the value published for $t_{20}^{\rm lab}(180°) \equiv T_{20}(180°)$ at 140 MeV (Ref. 5) we obtain an excitation function of $T_{20}(180°)$ between 134 and 294 MeV. This is illustrated in Fig. 12(a). The curves are the predictions from different theory groups, and are labelled as in Figs. 8 and 9. The circles represent our data, while the squares

TABLE III. Values of T_{20}, extrapolated to 180°.

T_π (MeV)	$T_{20}(180°)$
134	-0.50 ± 0.19
180	-1.02 ± 0.24
219	-1.26 ± 0.24
256	-0.74 ± 0.11
294	-0.85 ± 0.10

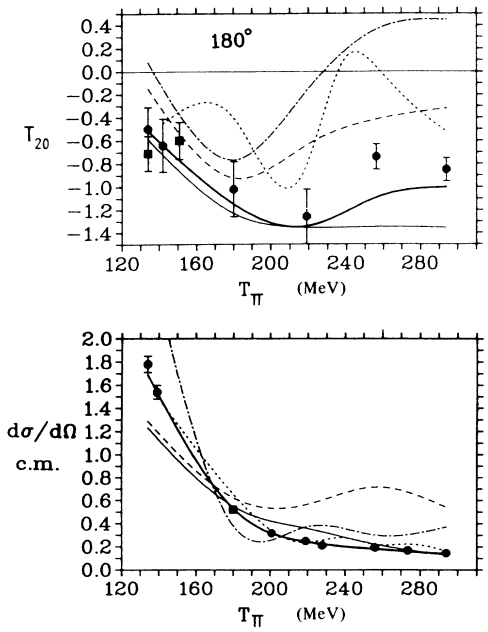

FIG. 12. Excitation function at 180° for (a) T_{20} and (b) $d\sigma/d\Omega$. The various curves are theoretical predictions, labeled as in Figs. 8 and 9, except for the heavy solid line, which is from Ref. 19.

represent the data of Refs. 5 and 8. The heavy solid line is the prediction from Ferreira *et al.*[19] (see next chapter). In Fig. 12(b) we show the excitation function of the differential cross section.

The tensor observable $T_{20}(180°)$ allows us to determine which particular helicity amplitudes and the partial waves are most sensitive to the P_{11} treatment. πd elastic scattering may be described by four complex helicity amplitudes A, B, C, D.[20] The observables which have been measured so far in πd elastic scattering are expressed in terms of these helicity amplitudes as follows:

$$\frac{d\sigma}{d\Omega} = \tfrac{1}{3}(2|A|^2+4|B|^2+2|C|^2+|D|^2) ,$$

$$iT_{11} = \sqrt{6}\,\mathrm{Im}[B^*(A-C+D)]/(3d\sigma/d\Omega) ,$$

$$T_{20} = \sqrt{2}(|A|^2+|C|^2-|B|^2-|D|^2)/(3d\sigma/d\Omega) ,$$

$$T_{21} = -\sqrt{6}\,\mathrm{Re}[B^*(A-C-D)]/(3d\sigma/d\Omega) ,$$

$$T_{22} = \sqrt{3}(2\,\mathrm{Re}(A^*C)-|B|^2)/(3d\sigma/d\Omega) .$$

Since the amplitudes A and B vanish at $\theta = 180°$ the tensor observable T_{20} reduces to the following expression:

$$T_{20}(180°) = \sqrt{2}\,\frac{|C|^2-|D|^2}{2|C|^2+|D|^2} . \tag{4}$$

The fact that experimentally $T_{20}(180°)$ is almost equal to $-\sqrt{2}$ at some energies means that $|C|^2 \ll |D|^2$. This is also the prediction of theories with small contributions from the pole and nonpole parts of the P_{11} amplitude. On the other hand, theories with large contributions have $|C|^2 \geq |D|^2$. Therefore, at 180°, we trace the P_{11} problem to the helicity amplitude C. The effects from the

treatment of the P_{11} channel modify mainly the $J=0$ and $J=1$ partial waves. Therefore, since the $J=0$ partial wave does not contribute to C (angular momentum selection rules) all the large effects produced by those theories, and seen at 180°, are almost exclusively due to the $J=1$ partial wave in $|C|$. From the excitation function of T_{20} and $d\sigma/d\Omega$ at 180°, one can extract the energy dependence of $|C(180°)|^2$ and $|D(180°)|^2$, model independently. This is shown in Fig. 13.

A possible solution of the P_{11} problem in πd scattering was suggested recently by Jennings.[21] In addition to the four time-ordered diagrams which are included in conventional calculations, effects of cancellation from four diagrams which differ only in the time ordering of the emission and absorption of the pions were discussed. A model calculation showed that large cancellations between some diagrams can occur for higher energies at backward scattering angles. Preliminary calculations where such diagrams were added to the Faddeev amplitudes from Blankleider[11] and from Rinat,[14] indicate that considerable improvements in the predictions of the differential cross section, the vector analyzing power iT_{11}, the tensor analyzing power T_{20}, and the tensor-polarization t_{20}^{lab}, can be obtained.

D. The $N\Delta$ interaction

In the energy region covered by our experiments pion-deuteron scattering proceeds predominantly through the excitation of intermediate Δ states, where Δ stands for any pion-nucleon isobar (including the P_{11}), with the main contribution coming from the P_{33} isobar. So, what are the uncertainties in the calculation of the πd elastic amplitude shown in Fig. 14? First, there is the dNN vertex, which is known as well as one knows the deuteron wave function, which means reasonably well. Secondly, the $\pi N\Delta$ vertex which, in the case of the diagram in Fig. 14, involves a pion on-the-mass shell and a nucleon off-the-mass shell. But this nucleon, since it is very heavy, is also almost on-the-mass-shell, so that the $\pi N\Delta$ vertex in Fig. 14 is almost the on-shell vertex which is well-known from the elementary pion-nucleon amplitudes. Thus, finally, we come to the third element, which is less well known, that is the $N\Delta \rightarrow N\Delta$ amplitude. The $N\Delta \rightarrow N\Delta$ amplitude is usually calculated within the Faddeev formalism, although there are some processes, involving a $\pi\Delta\Delta$ vertex or a crossed box diagram, etc., which are outside the scope of the Faddeev theory. Thus, the discrepancies between our data, and the predictions from a Faddeev calculation, are an indication of the importance of these non-Faddeev diagrams. Thus, by parametrizing this discrepancy in the form of a residual nucleon-delta interaction one may learn about this part of the nucleon-delta amplitude.

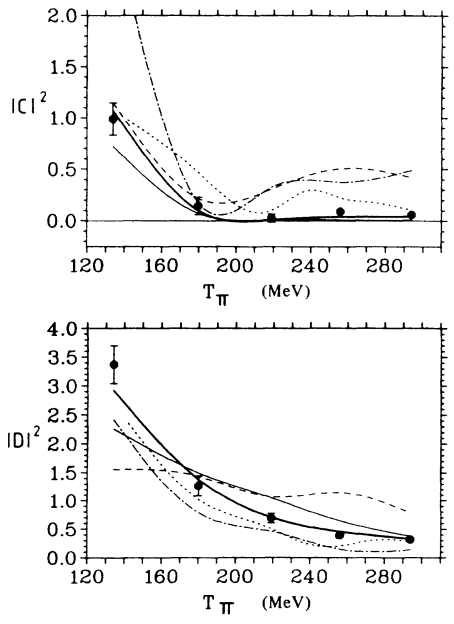

FIG. 13. Values of the helicity amplitudes $|C|^2$ and $|D|^2$ extracted from the experimental results for T_{20}, extrapolated to 180°. The curves represent various theoretical predictions, and are labeled as in Fig. 12.

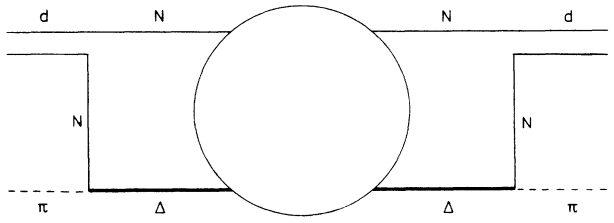

FIG. 14. Pictoral representation of the πd elastic scattering amplitude.

de Andrade *et al.*[22] tried to explain the persistent discrepancy between the theoretical predictions, and the large-angle cross section and iT_{11} data in terms of a short-range $N\Delta$ interaction. An $N\Delta$ model was constructed, the amplitudes of which were added to the Faddeev amplitudes of Rinat and Starkand,[14] and Mizutani *et al.*[23] Since it was not known beforehand which parameters of the $N\Delta$ interaction would prove to be relevant, they were treated as free parameters, and were determined from fitting all available data on the total cross section, the differential cross section and the vector analyzing power iT_{11}. In spite of the fact that a large number of $N\Delta$ partial waves was used in the search, it was not possible to fully overcome the discrepancy between the Faddeev calculations and the experimental data. However, it was shown that the $N\Delta$ interaction in the $^5S_2$ and $^5P_3$ waves gave important additional contributions, which resulted in remarkable improvements in the description of the data. Suspecting that the results of their analysis may depend on the choice of the Faddeev background amplitudes, the authors repeated their analysis,[19] this time starting with the recent Faddeev amplitudes of Garcilazo,[12] which provide a simultaneous description of the πd, NN, and πNN channels. Again a large number of partial waves were used in the search, and again only the $^5S_2$ and $^5P_3$ waves proved to be important. This time, however, the experimental data between 125 and 325 MeV was reproduced almost perfect-

ly. Although the required modifications of Garcilazo's amplitudes in the corresponding πd partial waves $^3P_2$ and $^3D_3$ were shown to be quite small, the effects on the observables where discrepancies were eliminated were quite strong. In the analysis of Ferreira *et al.*[19] the tensor observables were not included in the fitting procedure, but treated as predictions. In Fig. 15 we compare the predictions from Garcilazo (light solid line) with the predictions from Ferreira *et al.* (heavy solid line) for the observables T_{20}, T_{21}, and T_{22}. As one can see, the inclusion of the $N\Delta$ states produces a definite improvement for T_{20}. There is a factor of four reduction in χ^2 at 294 MeV, and a factor of 2 at 256 MeV. The other observables are not sensitive. In Fig. 13 the same comparison is made for the energy dependence of T_{20} at 180°. The effect of the $N\Delta$ states is very strong at the highest energies.

Strangely enough, the fits of Ferreira *et al.* for the πd observables did not require contributions from the $^3S_1$ $N\Delta$ state, which is the only other possible state with $L=0$ other than the $^5S_2$. The $^3S_1$ state should give a contribution $\frac{1}{3}$ the size of the one from the $^5S_2$ state, but it was not seen, within the accuracy of the experimental data. When utilizing our new data, however, in particular the much more precise values of iT_{11}, the $^3S_1$ state showed up as contributing $N\Delta$ state.[24] This state can only be reached by means of the reactions $\pi d \to \pi d$ or $\pi d \to \pi NN$, since it is forbidden for reactions involving an initial or final NN state. In Fig. 16 we display the phase shifts of the $^5S_2$ and $^5P_3$ waves as calculated from the amplitudes of Table I of Ref. 19, assuming the inelasticity $\eta=1$. The phase shifts of the $^3S_1$ wave are from the latest preliminary results.[24] For the $^5S_2$ and $^5P_3$ $N\Delta$ interaction there are also results from the isobar analysis of the $\gamma d \to \pi^- pp$ reaction,[25] and from the pion production reaction $pp \to \pi^+ pp$.[26] In spite of the large scatter of the phase shift data, a common trend is seen for the $^5S_2$ wave. The large discrepancy between the results of Ferreira *et al.*[19] and Shypit *et al.*[26] in the $^5P_3$ wave demonstrates the present accuracy with which one can extract $N\Delta$ phase shifts. The phase shift of the $^5S_2$ channel is positive, which means that the $N\Delta$ interaction in this channel is attractive. The phase shift of the $^3S_1$ channel, on the other hand, is negative, which means that the $N\Delta$ interaction is repulsive in that channel. Thus, since these two channels differ only in the fact that in the first one the spin of the nucleon and the spin of the Δ are parallel to each other, while in the second one the two spins are antiparallel, it follows that there is a strong spin-spin term in the $N\Delta$ interaction. Remember that the operator $\sigma_N \cdot \sigma_\Delta$ is equal to $\frac{3}{4}$ for the $^5S_2$ channel and $-\frac{5}{4}$ for the $^3S_1$ channel.

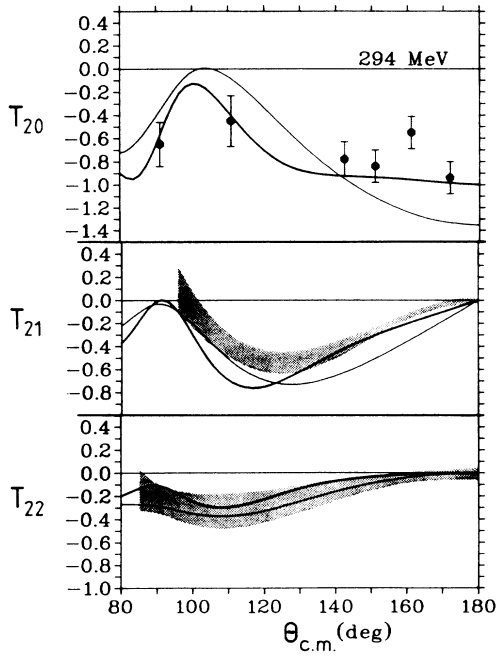

FIG. 15. Experimental results for T_{20} (solid circles) and T_{21}, T_{22} (shaded bands) at $T_\pi=294$ MeV, in comparison with theoretical predictions from Garcilazo (Ref. 12) (solid lines) and Ferreira *et al.* (Ref. 19) (heavy solid lines).

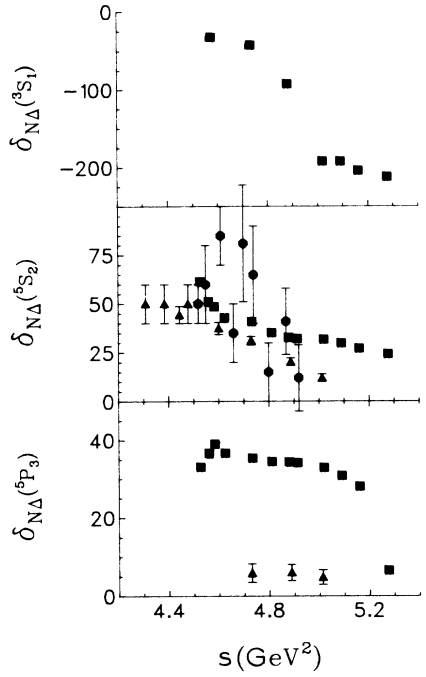

FIG. 16. The $N\Delta$ phase shifts for the lowest orbital angular momentum states, $^3S_1$, $^5S_2$, and $^5P_3$, as a function of the Mandelstam variable S. The squares are the results of Ferreira *et al.* (Refs. 19 and 24), the triangles are from Shypit *et al.* (Ref. 26), and the circles are from Laget (Ref. 25).

In conclusion one can state that independent of the details of the theoretical approach of Ferreira *et al.*, an $N\Delta$ interaction (possibly of short range) seems to be relevant to the πd scattering problem, and should be investigated further.

ACKNOWLEDGMENTS

The polarized target material was kindly provided by Dr. T. O. Niinikoski, European Organization for Nuclear

Research (CERN). This work would have been impossible without the generous help and considerable skills of the staff of SIN. It was supported by the Bundesministerium für Forschung und Technologie of the Federal Republic of Germany.

APPENDIX

We present a derivation of the connection between the tensor polarizations $t_{2k}^{\rm lab}$ and the tensor analyzing powers T_{2j} for the πd elastic scattering reaction. We use the notation defined by Grein and Locher.[20] In particular the tensor analyzing powers and polarizations are represented by

$$(2j \mid 00)=(-1)^j\cdot T_{2j} ,$$

$$(00 \mid 2k)=(-1)^k\cdot t_{2k} ,$$

and similarly for iT_{11} and it_{11}. The coordinate system used is defined following the Madison convention. The observables should be understood to be in the c.m. frame, as long as they are not explicitly specified as being in the lab frame. The following relationships are valid for the πd elastic scattering reaction, and follow from parity conservation and time reversal invariance, respectively:

$$(LM \mid L'M')=(-1)^{L+L'+M+M'}(L-M \mid L'-M') ,$$

$$(LM \mid L'M')=(-1)^{M+M'}(L'M' \mid LM) . \tag{5}$$

An additional relationship between the lab and and c.m. quantities is given by

$$(LM \mid L'M')^{\rm lab}=\sum_N (LM \mid L'N)d^{L'}_{NM'}(-\theta_R) , \tag{6}$$

where $\theta_R>0$ is the deuteron recoil angle in the lab frame, and d^j_{mn} is the Wigner d function. It has the following properties:

$$d^j_{nm}=(-1)^{m-n}d^j_{mn}=d^j_{-m-n} ,$$

$$d^j_{mn}(-\alpha)=(-1)^{n+m}d^j_{mn}(\alpha) .$$

Since $d^0_{00}=1$, Eq. (6) implies that the analyzing powers measured in the lab frame are identical to those in the c.m. frame. In addition, because of time reversal invariance, it can be shown that

$$iT_{11}^{\rm lab}=iT_{11}=it_{11}$$

and

$$T_{2j}^{\rm lab}=T_{2j}=(-1)^j t_{2j} .$$

While the vector polarization $it_{11}^{\rm lab}$ of the recoil deuterons is still determined directly by the c.m. value (i.e., $it_{11}^{\rm lab}=it_{11}$), the tensor polarizations $t_{2k}^{\rm lab}$ are linear combinations of all c.m. tensor analyzing powers. Using Eq. (5), it can be shown that

$$t_{2-k}^{\rm lab}=(-1)^k t_{2k}^{\rm lab} .$$

Therefore, only three lab polarizations have to be calculated. By combining these relationships, one can derive that

$$t_{2k}^{\rm lab}=(-1)^k\left[T_{20}d^2_{k0}(\theta_R) + \sum_{m=1}^{2} T_{2m}[\, d^2_{km}(\theta_R) +(-1)^m d^2_{k-m}(\theta_R)]\right] . \tag{7}$$

This equation can be rewritten as a 3×3 matrix:

$$\begin{pmatrix} t_{20} \\ t_{21} \\ t_{22} \end{pmatrix}^{\rm lab} =[\alpha_{km}] \begin{pmatrix} T_{20} \\ T_{21} \\ T_{22} \end{pmatrix} , \tag{8}$$

where

$$\alpha_{k0}=(-1)^k d^2_{k0}(\theta_R) ,$$

$$\alpha_{km}=(-1)^k[d^2_{km}(\theta_R)+(-1)^m d^2_{k-m}(\theta_R)], \quad m=1,2 .$$

The transformation from the lab tensor polarizations to the c.m. analyzing powers can be easily obtained by inverting the above matrix. The explicit values of the matrix have been given in the main part of the text.

[1] C. R. Ottermann *et al.*, Phys. Rev. C **38**, 2296 (1988).

[2] J. Bolger *et al.*, Phys. Rev. Lett. **46**, 167 (1981); **48**, 1667 (1982); E. L. Mathie *et al.*, Phys. Rev. C **28**, 2258 (1983); G. R. Smith *et al.*, *ibid.* **29**, 2206 (1984).

[3] H. Garcilazo *et al.* (unpublished).

[4] R. J. Holt *et al.*, Phys. Rev. Lett. **43**, 1229 (1979); **47**, 472 (1981).

[5] E. Ungricht *et al.*, Phys. Rev. Lett. **52**, 333 (1984); Phys. Rev. C **31**, 934 (1985).

[6] J. Ulbricht *et al.*, Phys. Rev. Lett. **48**, 311 (1982); W. Grüebler *et al.*, *ibid.* **49**, 444 (1982); V. Koenig *et al.*, J. Phys. G **69**, L211 (1983).

[7] Y. M. Shin *et al.*, Phys. Rev. Lett. **55**, 2672 (1985).

[8] G. R. Smith *et al.*, Phys. Rev. Lett. **57**, 803 (1986).

[9] G. R. Smith *et al.*, Phys. Rev. C **38**, 251 (1988).

[10] C. Fayard, G. H. Lamot, and T. Mizutani, Phys. Rev. Lett. **45**, 524 (1980); G. H. Lamot *et al.*, Phys. Rev. C **35**, 239 (1987).

[11] B. Blankleider and I. R. Afnan, Phys. Rev. C **24**, 1572 (1981).

[12] H. Garcilazo, Phys. Rev. Lett. **53**, 652 (1984); Phys. Rev. C **35**, 1820 (1987).

[13] H. Pöpping, P. V. Sauer, and Zhang Xi-Zhen, Nucl. Phys. **A474**, 557 (1987).

[14] A. S. Rinat and Y. Starkand, Nucl. Phys. **A397**, 381 (1983).

[15] T.-S. H. Lee and A. Matsuyama, Phys. Rev. C **36**, 1459 (1987).

[16] M. Betz and T.-S. H. Lee, Phys. Rev. C **23**, 375 (1981).

[17] H. Garcilazo, in *Few Body Systems*, Suppl. 1, edited by C. Ciofi degli Atti, O. Benhar, E. Pace, and G. Salmè (Springer-Verlag, New York, 1986), p. 456.

[18] I. R. Afnan and R. J. McLeod, Phys. Rev. C **31**, 1821 (1985).

[19]E. Ferreira, S. C. B. de Andrade, and H. G. Dosch, Phys. Rev. C **36**, 1916 (1987).
[20]W. Grein and M. P. Locher, J. Phys. G **7**, 1355 (1981).
[21]B. Jennings, Phys. Lett. B **205**, 187 (1988).
[22]S. C. B. de Andrade, E. Ferreira, and H. G. Dosch, Phys. Rev. C **34**, 226 (1986).
[23]T. Mizutani *et al.*, Phys. Rev. C **24**, 2633 (1981); Phys. Lett. **107B**, 177 (1981).
[24]E. Ferreira and H. G. Dosch, Phys. Rev. C (in press); E. Ferreira, private communication.
[25]J. M. Laget, in *New Vistas in Electro-Nuclear Physics,* edited by E. L. Tomusiak, H. S. Caplan, and E. T. Dressler (Plenum, New York, 1986), p. 361.
[26]R. L. Shypit, Phys. Rev. Lett. **60**, 901 (1988).

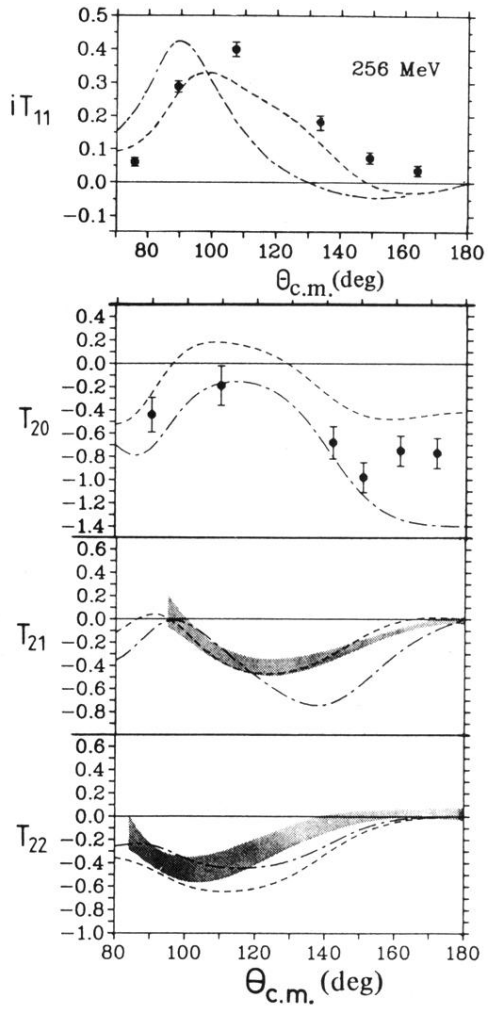

FIG. 10. Experimental results for iT_{11}, T_{20} (solid circles), and T_{21}, T_{22} (shaded bands) at $T_\pi = 256$ MeV. The dashed and dot-dashed curves are the theoretical predictions of Ref. 11, with and without the P_{11} amplitude, respectively.

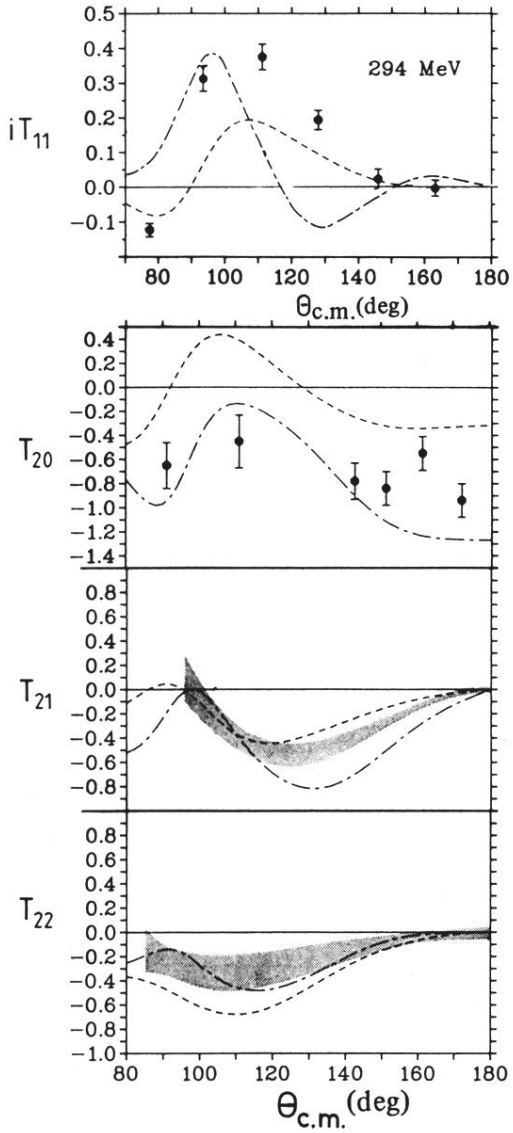

FIG. 11. Same as Fig. 10, but for $T_\pi = 294$ MeV.

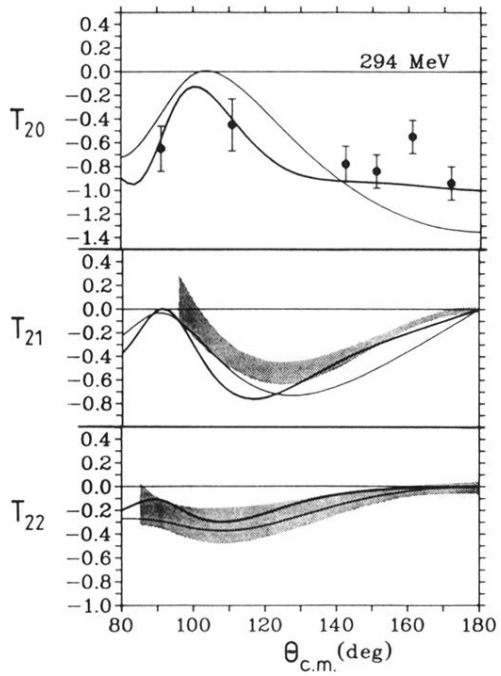

FIG. 15. Experimental results for T_{20} (solid circles) and T_{21}, T_{22} (shaded bands) at $T_\pi = 294$ MeV, in comparison with theoretical predictions from Garcilazo (Ref. 12) (solid lines) and Ferreira *et al.* (Ref. 19) (heavy solid lines).

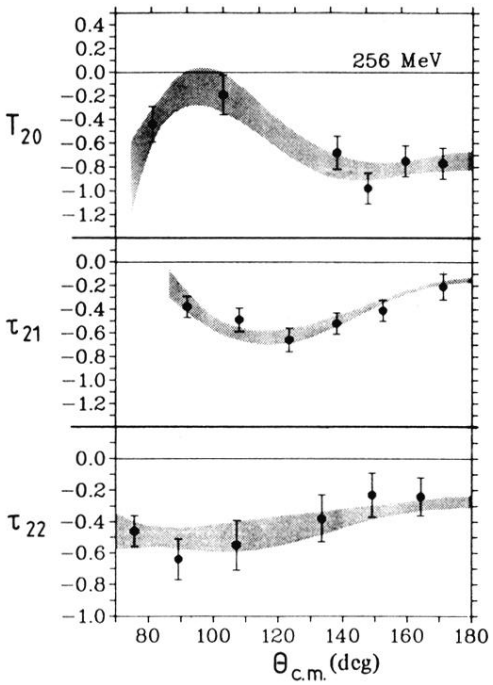

FIG. 6. Present results for τ_{22} at $T_\pi = 256$ MeV, along with the results for T_{20} and τ_{21} from part I of this paper (Ref. 1). The shaded bands represent the results of a Legendre polynomial fit to the data, which included the mean of the values extrapolated to 180° as one of the fitted points.

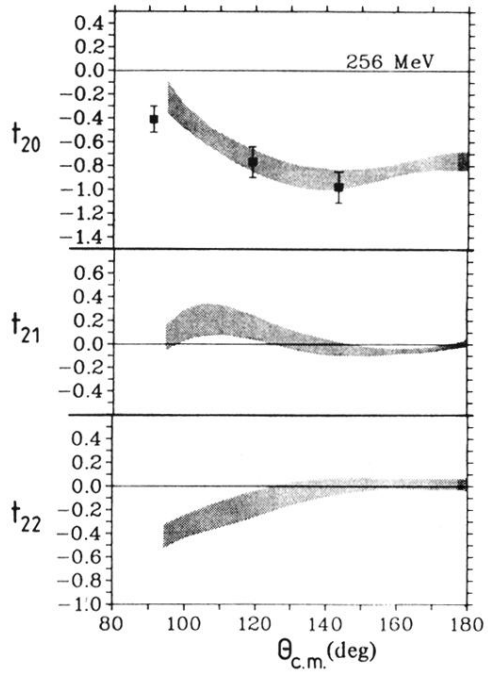

FIG. 7. The shaded bands represent values of t_{20}^{lab}, t_{21}^{lab}, and t_{22}^{lab} determined from a fit to our measured values of T_{20}, τ_{21}, and τ_{22}. The data points are from Ref. 5.